

VIRTUAL PROTOTYPING, DESIGN AND ANALYSIS OF AN IN-PIPE INSPECTION MOBILE ROBOT

MICHAŁ CISZEWSKI, TOMASZ BURATOWSKI, MARIUSZ GIERGIEL, PIOTR MAŁKA

*AGH University of Science and Technology, Faculty of Mechanical Engineering and Robotics, Kraków, Poland
e-mail: mcisz@agh.edu.pl; tburatow@agh.edu.pl; giergiel@agh.edu.pl; malka@agh.edu.pl*

KRZYSZTOF KURC

*Rzeszow University of Technology, Faculty of Mechanical Engineering and Aeronautics, Rzeszów, Poland
e-mail: kkurc@prz.edu.pl*

This paper presents a design of a tracked in-pipe inspection mobile robot with a flexible drive positioning system. The robot is intended to operate in circular and rectangular pipes and ducts oriented horizontally and vertically. The paper covers the complete design process of a virtual prototype, focusing on track adaptation to the working environment. A mathematical description of kinematics and dynamics of the robot is presented. Operation in pipes with a cross section over 210 mm is discussed. Laboratory tests of the utilized tracks are included, confirming conducted FEA simulations.

Keywords: pipeline inspection, mobile robot, drive positioning, Maggi's equations

1. Introduction

Pipeline inspection is a popular application field of mobile robots. Since access to a particular segment of a pipeline is usually limited; various in-pipe inspection mobile robots are utilized. This paper presents a design of a tracked mobile robot that can adapt to various working environments. The robot platform is based on two track modules with integrated motors, mounted on the positioning structure, consisting of three drives per track. The robot would be able to operate in pipes and ducts with round and rectangular cross-sections oriented horizontally and vertically or to work on flat surfaces. Application of a flexible track positioning system would allow on-line changes of the robot structure.

There already exist many other designs of mobile pipe inspection robots, but the majority of them possesses low level of adaptivity to the operating environment, mainly due to geometric limitations. Choi and Roh (2007) focused on design of wheeled inspection robots suitable for $\emptyset 200$ and $\emptyset 85-109$ mm round pipes that are based on a modular structure that features segments with wheeled legs on pantograph mechanisms for diameter changes. Another concept was presented by Horodincea *et al.* (2002). They designed four robot architectures utilizing a rotor equipped with three pairs of tilted wheels moving on helical trajectories, propelling the robot forwards in the axial direction. The robots had different sizes for 170, 70 and 40 mm round pipes and allow only small changes of the diameter. Tadakuma *et al.* (2009) proposed a platform with a cylindrical track drive – Omni-Track that increases the contact area with pipes of different diameters and allow forward and backward motions along with side motion realized by a roll mechanism. A three-track vertical configuration for a constant pipe diameter was described.

Robots for operation in ventilation ducts are mainly designed with focus on cleaning tasks. Wang and Zhang (2006) proposed a tracked platform with a guiding wheel, intended for operation with interchangeable brushes for horizontal ducts.

The market for inspection robots offers several solutions. Inuktun produces a wide range of tracked inspection robots. Versatrax models are available in three different sizes for minimal

pipe diameters: 100, 150 and 300 mm (Inuktun, 2012). Their main components are individually operated tracks of different sizes. Manually adjustable chassis allows adapting of the robot to sewer and storm drains, air ducts, tanks, oil and gas pipelines, pulp and paper industries. Versatrax Vertical is a three-track version for a vertical, dry pipe inspection (Hydropulsion, 2012). iPEK produces wheeled inspection vehicles ROVVER for pipes with diameters 100-300, 150-760 and 230-1520 mm (Ipek, 2011). These robots have modular designs with replaceable wheels, suitable for horizontal pipes and operation up to 10 m underwater. A Solo robot by RedZone is a tracked, wireless, autonomous robot that can be used in pipes ranging from 200-300 mm diameters (Redzone, 2012). CUES offers tracked inspection robots for pipes that vary from 150 to 760 mm. Their main feature is a narrow track made of large segments (Cues, 2012).

As we may observe, numerous solutions for inspection robots are available. Wheels provide the least rolling resistance and are energy efficient, however a small contact surface may not be sufficient for some uneven surfaces. Crawling motion has speed limitations, and especially the upper limit of a pipe or duct dimension is the major drawback. As presented by market research, numerous solutions utilizing track drives have been developed. Tracks provide proper obstacle avoidance capabilities and a considerably large contact area. Sufficient contact surface is an advantage in terms of friction. The presented tracked robots do not possess online track positioning and are designed for specific purposes. This paper presents a design of a versatile tracked mobile robot with an adaptive track positioning system intended for video inspection.

2. Mechanical structure

Similarly to most of the analyzed robots structures, it was decided to utilize two tracks. That configuration ensures proper robot stability and maneuverability, assuming that the robot will consist of one segment. For this project, Inuktun Microtrac track modules with dimensions $60 \times 50 \times 170$ mm are analysed. They are designed specifically for pipe inspection, with focus on small inspection platforms. For creation of a virtual prototype of the inspection robot, Autodesk Inventor Professional 2012 was used.

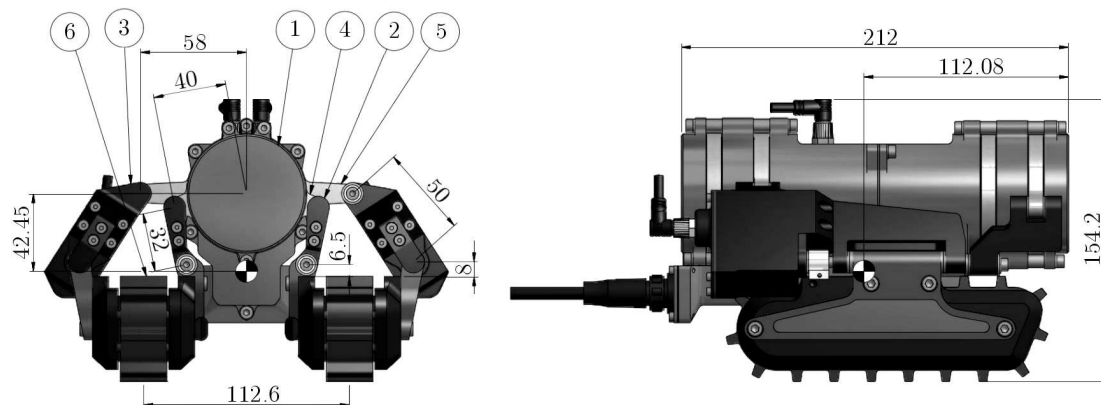


Fig. 1. Robot model – general view; 1 – robot body, 2 – front arm, 3 – rear arm, 4 – front rotating ring, 5 – rear rotating ring, 6 – track drive unit

The track positioning system consists of two independently rotating rings with the centre of rotation in the axis of the robot body. To each of these rings, an arm is attached on a rotary joint. These arms are similarly mounted to both sides of each track. This configuration allows various orientations of the tracks with respect to the robot body. Each track unit is adjusted by three drives. Two drives allow rotations of rings with respect to the robot body axis, and the third drive positions one arm with respect to the track. The drives selected for the rotating rings

are digital servomotors Hitec HS-7950TH that are compact size, possess high holding torque and an integrated position controller. The rotating rings are connected with the outer and inner arms of the robot.

The general view of the robot is presented in Fig. 1. The drive controllers and power electronics are located inside the robot body.

In total, the robot has 8 drives: 2 tracks and 6 track positioning servomotors and consists of over 230 components, among which over 60 have to be manufactured. The total weight of the robot is 5.14 kg, where the weight of one aluminum track is 1.1 kg. The total weight does not include camera, lighting and cables. The robot is capable of operating in liquid environment such as water, sewage or oil. In order to meet this requirement, connections are sealed and cables are routed with usage of waterproof connectors.

3. Kinematic model of the robot

The description a crawler track in a real environment with uneven ground and changeable conditions is very complex. The detailed mathematical description of movement of individual crawler track points is so compound that it is necessary to apply simplified models. Elastomer tracks with treads could be modeled as a non-stretch tape wound about a determined shape by a drive sprocket, an idler and an undeformable ground (Burdziński, 1972; Dajniak, 1985; Trojnecki, 2011; Żylski, 1996). The presented kinematic model of the robot describes a plane motion and operation on inclined surfaces.

The velocity of the point C (Fig. 2a), placed in the axis of symmetry of the crawler (Burdziński, 1972; Chodkowski, 1982, 1990; Dajniak, 1985; Żylski, 1996) may be expressed as

$$V_c = \sqrt{\dot{x}_C^2 + \dot{y}_C^2 + \dot{z}_C^2} \quad (3.1)$$

The equations for particular velocity components were derived taking into consideration slip of the tracks and an assumption that the principal direction of motion is the y axis, and the angle of turn β is positive towards the x axis (Fig. 2a)

$$\begin{aligned} \dot{x}_C &= \frac{r\dot{\alpha}_1(1-s_1) + r\dot{\alpha}_2(1-s_2)}{2} \sin \beta & \dot{y}_C &= \frac{r\dot{\alpha}_1(1-s_1) + r\dot{\alpha}_2(1-s_2)}{2} \cos \beta \cos \gamma \\ \dot{z}_C &= \frac{r\dot{\alpha}_1(1-s_1) + r\dot{\alpha}_2(1-s_2)}{2} \sin \gamma & \dot{\beta} &= \frac{r\dot{\alpha}_2(1-s_2) - r\dot{\alpha}_1(1-s_1)}{H} \end{aligned} \quad (3.2)$$

where r is the radius of the track drive sprockets, H – distance between the tracks, s_1 – slip of sprocket 1, s_2 – slip of the sprocket 2, G – gravity force, η – efficiency, $\dot{\alpha}_1$ – angular velocity of sprocket 1, $\dot{\alpha}_2$ – angular velocity of sprocket 2, γ – angle of slope inclination.

The slip of the track is calculated using the following formula

$$s = \frac{(n-1)dL}{L} \quad (3.3)$$

where n is the number of track treads in contact with the ground, dL – track tread deformation, L – length of the track load bearing segment.

The velocities of the points V_F and V_G , located in the centers of + tracks may be expressed as

$$V_F^2 = \dot{x}_F^2 + \dot{y}_F^2 + \dot{z}_F^2 \quad V_G^2 = \dot{x}_G^2 + \dot{y}_G^2 + \dot{z}_G^2 \quad (3.4)$$

$$\dot{x}_F = \dot{x}_C - \frac{1}{2}H\dot{\beta} \sin \beta \quad \dot{y}_F = \dot{y}_C - \frac{1}{2}H\dot{\beta} \cos \beta \quad \dot{z}_F = \dot{z}_C \quad (3.5)$$

$$\dot{x}_G = \dot{x}_C + \frac{1}{2}H\dot{\beta} \sin \beta \quad \dot{y}_G = \dot{y}_C + \frac{1}{2}H\dot{\beta} \cos \beta \quad \dot{z}_G = \dot{z}_C \quad (3.6)$$

The created kinematic model will be used in determination of dynamical equations of motion.

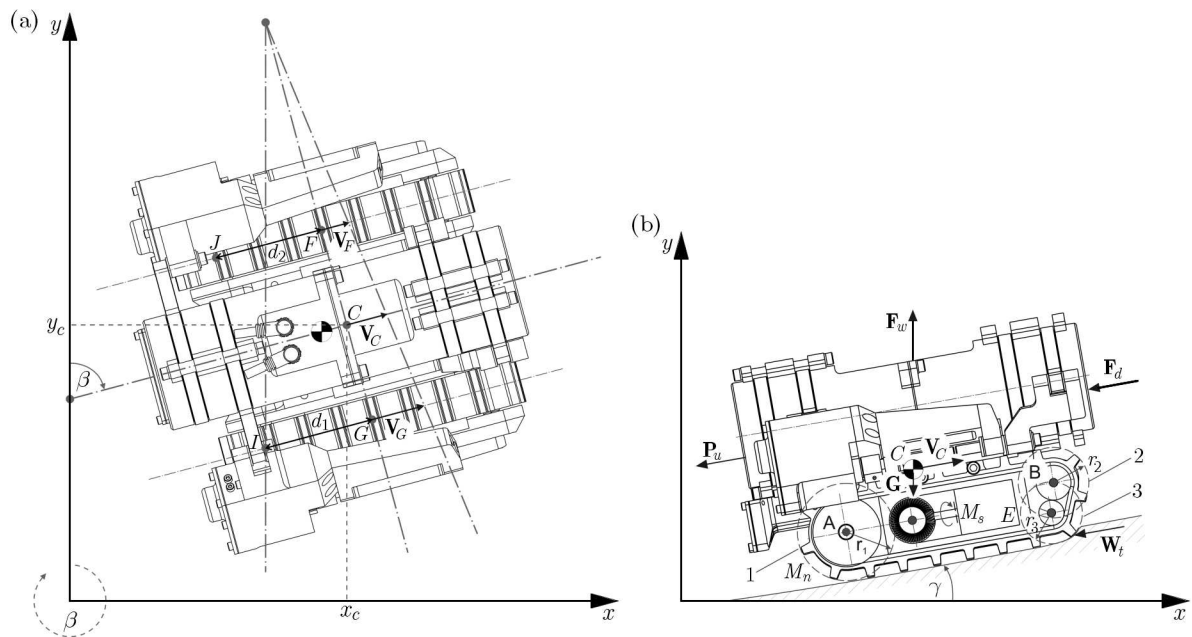


Fig. 2. Robot frame rotated by the angle β (a) and dynamic model of the robot – forces (b)

4. Dynamic model of the inspection robot

The dynamic description of the robot (Burdziński, 1972; Chodkowski, 1982, 1990; Dajniak, 1985; Trojnacki, 2011; Żylski, 1996) was prepared using an energetic method based on Lagrange equations. In order to avoid modeling problems with decoupling Lagrange multipliers, Maggi's equations were used (Giergiel and Żylski, 2005). In the dynamic model of the robot, the same characteristic points on the structure are considered as in the kinematic description (Fig. 3).

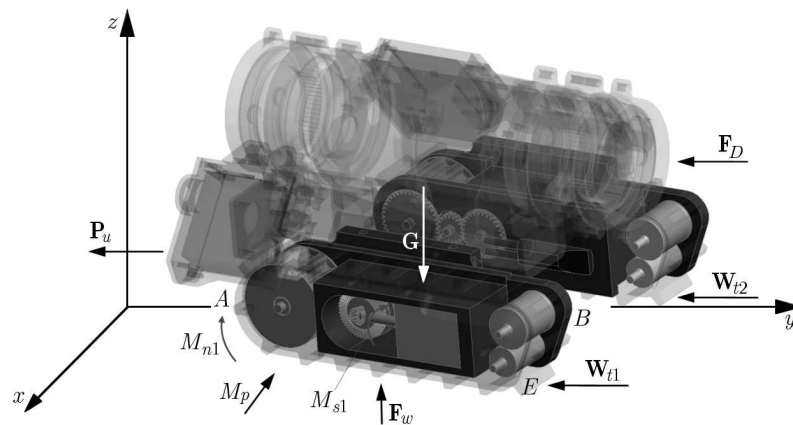


Fig. 3. Dynamic model of the robot – forces acting on the robot

It has to be assumed that the kinetic energy of the robot E is the sum of energies of particular components

$$E = E_R + E_{M1} + E_{M2} \quad (4.1)$$

where E_R is the kinetic energy of the robot frame, E_{M1} – kinetic energy of the left track drive module, E_{M2} – kinetic energy of the right track drive module.

The kinetic energy of the robot frame is the sum of energies E_{R1} and E_{R2} , resultant from translational and rotational motion with respect to the instantaneous center of rotation O

$$E_R = E_{R1} + E_{R2} = \frac{1}{2}m_R V_C^2 + \frac{1}{2}I_R \dot{\beta}^2 \quad (4.2)$$

where m_R is the mass of the robot frame, I_R – moment of inertia of the robot frame, $\dot{\beta}$ – angular velocity of the robot frame with respect to the instantaneous center of rotation.

By introducing equation (4.2) into (3.1), the kinetic energy of the robot frame was obtained

$$E_R = \frac{1}{2}m_R(\dot{x}_C^2 + \dot{y}_C^2 + \dot{z}_C^2) + \frac{1}{2}I_R \dot{\beta}^2 \quad (4.3)$$

The kinetic energy of the track drive module was determined by making use of the following formula

$$E_M = E_{K1} + E_{K2} + E_{K3} + E_O \quad (4.4)$$

where E_{K1} is the kinetic energy of track drive sprocket 1, E_{K2} – kinetic energy of idler 2, E_{K3} – kinetic energy of idler 3, E_O – kinetic energy of the track module housing.

The kinetic energy of the sprocket and idlers in the track module can be expressed as a sum of kinetic energies of translational motion, rotational motion about the particular axis of rotation and rotational motion about the instantaneous center of rotation (Giergiel *et al.*, 2012). The moments of inertia were determined for the particular models of the sprocket and idlers that were modeled in a CAD software, according to the datasheet from the Inuktun company (Inuktun, 2012)

$$\begin{aligned} E_{K1} &= \frac{1}{2}m_{K1}V_A^2 + \frac{1}{2}I_{x1}\dot{\alpha}_{K1}^2 + \frac{1}{2}I_{z1}\dot{\beta}^2 & E_{K2} &= \frac{1}{2}m_{K2}V_B^2 + \frac{1}{2}I_{x2}\dot{\alpha}_{K2}^2 + \frac{1}{2}I_{z2}\dot{\beta}^2 \\ E_{K3} &= \frac{1}{2}m_{K3}V_E^2 + \frac{1}{2}I_{x3}\dot{\alpha}_{K3}^2 + \frac{1}{2}I_{z3}\dot{\beta}^2 \end{aligned} \quad (4.5)$$

where m_{Ki} is the mass of the i -th wheel, I_{xi} – moment of inertia with respect to the i -th axis of rotation x , I_{zi} – moment of inertia of the i -th wheel with respect to the axis z about which the wheel changes its orientation with the angular velocity $\dot{\beta}$, $\dot{\alpha}_{Ki}$ – angular velocity of the i -th wheel, V_A, V_B, V_E – velocities of characteristic points presented in Fig. 2a.

The kinetic energy of the track module housing is the sum of energies of the motor, gear transmission and the track

$$E_O = \frac{1}{2}m_O V_O^2 + \frac{1}{2}I_{xO}\dot{\alpha}_1^2 + \frac{1}{2}I_{zO}\dot{\beta}^2 \quad (4.6)$$

where m_O is the mass of the track module housing, I_{xO} – moment of inertia of the elements in rotational motion, I_{zO} – moment of inertia of the housing with respect to the instantaneous center of rotation.

The total kinetic energy of one track drive module is denoted as follows

$$\begin{aligned} E_M &= \frac{1}{2}m_{K1}V_A^2 + \frac{1}{2}I_{x1}\dot{\alpha}_{K1}^2 + \frac{1}{2}I_{z1}\dot{\beta}^2 + \frac{1}{2}m_{K2}V_B^2 + \frac{1}{2}I_{x2}\dot{\alpha}_{K2}^2 + \frac{1}{2}I_{z2}\dot{\beta}^2 \\ &+ \frac{1}{2}m_{K3}V_E^2 + \frac{1}{2}I_{x3}\dot{\alpha}_{K3}^2 + \frac{1}{2}I_{z3}\dot{\beta}^2 + \frac{1}{2}m_O V_O^2 + \frac{1}{2}I_{xO}\dot{\alpha}_1^2 + \frac{1}{2}I_{zO}\dot{\beta}^2 \end{aligned} \quad (4.7)$$

with the assumption that

$$V_A = V_B = V_E = V_O = V \quad (4.8)$$

and

$$E_M = \frac{1}{2}V^2(m_{K1} + m_{K2} + m_{K3} + m_O) + \frac{1}{2}I_{x1}\dot{\alpha}_{K1}^2 + \frac{1}{2}I_{x2}\dot{\alpha}_{K2}^2 + \frac{1}{2}I_{x3}\dot{\alpha}_{K3}^2 + \frac{1}{2}I_{xO}\dot{\alpha}_1^2 + \frac{1}{2}\dot{\beta}^2(I_{z1} + I_{z2} + I_{z3} + I_{zO}) \quad (4.9)$$

When taking into account the relations between angular velocities and radii of the sprocket and idlers

$$\alpha_{K1}r_1 = \alpha_{K2}r_2 = \alpha_{K3}r_3 = \alpha_1 r \quad \dot{\alpha}_1 r_{K1} = \dot{\alpha}_{K2}r_2 = \dot{\alpha}_{K3}r_3 = \dot{\alpha}_1 r \quad (4.10)$$

Thus, using the following substitution

$$m = m_{K1} + m_{K2} + m_{K3} + m_O \quad I_x = I_{x1} + I_{x2}\left(\frac{r_1}{r_2}\right)^2 + I_{x3}\left(\frac{r_1}{r_3}\right)^2 + I_{xO} \quad (4.11)$$

$$I_z = I_{z1} + I_{z2} + I_{z3} + I_{zO}$$

The total kinetic energy for the track drive module is derived

$$E_M = \frac{1}{2}mV^2 + \frac{1}{2}I_x\dot{\alpha}_1^2 + \frac{1}{2}I_z\dot{\beta}^2 \quad (4.12)$$

Previously, only one track drive module was investigated and particular properties were denoted without an index. However, in a more detailed analysis, the energy of the left and right track drive module is used (according to the notation in Fig. 2a)

$$E_{M1} = \frac{1}{2}mV_F^2 + \frac{1}{2}I_x\dot{\alpha}_1^2 + \frac{1}{2}I_z\dot{\beta}^2 \quad E_{M2} = \frac{1}{2}mV_G^2 + \frac{1}{2}I_x\dot{\alpha}_2^2 + \frac{1}{2}I_z\dot{\beta}^2 \quad (4.13)$$

After substitution of velocities denoted in (3.4), the following formulas are obtained

$$E_{M1} = \frac{1}{2}m[(\dot{x}_C - \dot{\beta}H \sin \beta)^2 + (\dot{y}_C - \dot{\beta}H \cos \beta)^2 + \dot{z}_C^2] + \frac{1}{2}I_x\dot{\alpha}_1^2 + \frac{1}{2}I_z\dot{\beta}^2 \quad (4.14)$$

$$E_{M2} = \frac{1}{2}m[(\dot{x}_C + \dot{\beta}H \sin \beta)^2 + (\dot{y}_C + \dot{\beta}H \cos \beta)^2 + \dot{z}_C^2] + \frac{1}{2}I_x\dot{\alpha}_2^2 + \frac{1}{2}I_z\dot{\beta}^2$$

The total kinetic energy of the robot described in (4.1) was derived by making use of equations (4.3) and (4.14)

$$E = \frac{1}{2}m_R(\dot{x}_C^2 + \dot{y}_C^2 + \dot{z}_C^2) + \frac{1}{2}I_R\dot{\beta}^2 + \frac{1}{2}m[(\dot{x}_c - \dot{\beta}H \sin \beta)^2 + (\dot{y}_C - \dot{\beta}H \cos \beta)^2 + \dot{z}_C^2] + \frac{1}{2}I_x\dot{\alpha}_1^2 + I_z\dot{\beta}^2 + \frac{1}{2}m[(\dot{x}_C + \dot{\beta}H \sin \beta)^2 + (\dot{y}_C + \dot{\beta}H \cos \beta)^2 + \dot{z}_C^2] + \frac{1}{2}I_x\dot{\alpha}_2^2 \quad (4.15)$$

In order to determine the dynamic equations of motion, Maggi's formalism is employed

$$\sum_{j=1}^n C_{ij} \left[\frac{d}{dt} \left(\frac{\partial E}{\partial \dot{q}_j} \right) - \left(\frac{\partial E}{\partial q_j} \right) \right] = \theta_i \quad \dot{q}_j = \sum_{i=1}^s C_{ij} \dot{e}_i + G_j \quad (4.16)$$

where n denotes the number of independent parameters expressed by generalized coordinates q_i ($j = 1, \dots, n$) where according to Maggi's formalism

$$\dot{e} = [\dot{\alpha}_1, \dot{\alpha}_2]^T \quad \mathbf{G}_j = [0, 0, 0, 0, 0, 0]^T \quad (4.17)$$

According to this assumption, six generalized velocities were denoted by multiplication of the matrix C_{ij} that consists of nonholonomic constraints with two kinematic parameters $\dot{\alpha}_1, \dot{\alpha}_2$

$$\begin{bmatrix} \dot{x}_C \\ \dot{y}_C \\ \dot{z}_C \\ \dot{\beta} \\ \dot{\alpha}_1 \\ \dot{\alpha}_2 \end{bmatrix} = \begin{bmatrix} \frac{1}{2}r(1-s_1)\sin\beta & \frac{1}{2}r(1-s_2)\sin\beta \\ \frac{1}{2}r(1-s_1)\cos\beta\cos\gamma & \frac{1}{2}r(1-s_2)\cos\beta\cos\gamma \\ \frac{1}{2}r(1-s_1)\sin\gamma & \frac{1}{2}r(1-s_2)\sin\gamma \\ -\frac{r(1-s_1)}{H} & \frac{r(1-s_2)}{H} \\ 1 & 0 \\ 0 & 1 \end{bmatrix} \begin{bmatrix} \dot{\alpha}_1 \\ \dot{\alpha}_2 \end{bmatrix} \quad (4.18)$$

The generalized forces and moments are denoted as follows

$$\theta_i = \begin{bmatrix} M_{n1} + \left(-\frac{1}{2}P_u - \frac{1}{2}F_D - \frac{1}{2}G\sin\gamma + \frac{1}{2}F_w\sin\gamma - \frac{1}{2}W_{t1}\right)r(1-s_1) + M_p\frac{r(1-s_1)}{H} \\ M_{n2} + \left(-\frac{1}{2}P_u - \frac{1}{2}F_D - \frac{1}{2}G\sin\gamma + \frac{1}{2}F_w\sin\gamma - \frac{1}{2}W_{t2}\right)r(1-s_2) - M_p\frac{r(1-s_2)}{H} \end{bmatrix} \quad (4.19)$$

The final form of the dynamic equations of motion based on Maggi's formalism are presented as follows

$$\begin{aligned} & \left\{ \frac{r}{2}[\ddot{\alpha}_1(1-s_1) + \ddot{\alpha}_2(1-s_2)]\sin\beta + \frac{r}{2}[\dot{\alpha}_1(1-s_1) + \dot{\alpha}_2(1-s_2)] \right. \\ & \quad \left. \cdot \frac{r\dot{\alpha}_2(1-s_2) - r\dot{\alpha}_1(1-s_1)}{H}\cos\beta \right\} (m_R + 2m)\frac{1}{2}r(1-s_1)\sin\beta \\ & + \left\{ \frac{r}{2}[\ddot{\alpha}_1(1-s_1) + \ddot{\alpha}_2(1-s_2)]\cos\beta\cos\gamma - \frac{r}{2}[\dot{\alpha}_1(1-s_1) + \dot{\alpha}_2(1-s_2)] \right. \\ & \quad \left. \cdot \frac{r\dot{\alpha}_2(1-s_2) - r\dot{\alpha}_1(1-s_1)}{H}\sin\beta\cos\gamma \right\} (m_R + 2m)\frac{1}{2}r(1-s_1)\cos\beta\cos\gamma \\ & + \left\{ \frac{r}{2}[\ddot{\alpha}_1(1-s_1) + \ddot{\alpha}_2(1-s_2)]\sin\gamma \right\} (m_R + 2m)\frac{1}{2}r(1-s_1)\sin\gamma \\ & - \frac{r\ddot{\alpha}_2(1-s_2) - r\ddot{\alpha}_1(1-s_1)}{H}(I_R + 2I_z + 2mH^2)\frac{r(1-s_1)}{H} + I_x\ddot{\alpha}_1 \\ & = M_{n1} + \left(-\frac{1}{2}P_u - \frac{1}{2}F_D - \frac{1}{2}G\sin\gamma + \frac{1}{2}F_w\sin\gamma - \frac{1}{2}W_{t1}\right)r(1-s_1) + M_p\frac{r(1-s_1)}{H} \quad (4.20) \\ & \left\{ \frac{r}{2}[\ddot{\alpha}_1(1-s_1) + \ddot{\alpha}_2(1-s_2)]\sin\beta + \frac{r}{2}[\dot{\alpha}_1(1-s_1) + \dot{\alpha}_2(1-s_2)] \right. \\ & \quad \left. \cdot \frac{r\dot{\alpha}_2(1-s_2) - r\dot{\alpha}_1(1-s_1)}{H}\cos\beta \right\} (m_R + 2m)\frac{1}{2}r(1-s_2)\sin\beta \\ & + \left\{ \frac{r}{2}[\ddot{\alpha}_1(1-s_1) + \ddot{\alpha}_2(1-s_2)]\cos\beta\cos\gamma - \frac{r}{2}[\dot{\alpha}_1(1-s_1) + \dot{\alpha}_2(1-s_2)] \right. \\ & \quad \left. \cdot \frac{r\dot{\alpha}_2(1-s_2) - r\dot{\alpha}_1(1-s_1)}{H}\sin\beta\cos\gamma \right\} (m_R + 2m)\frac{1}{2}r(1-s_2)\cos\beta\cos\gamma \\ & + \left\{ \frac{r}{2}[\ddot{\alpha}_1(1-s_1) + \ddot{\alpha}_2(1-s_2)]\sin\gamma \right\} (m_R + 2m)\frac{1}{2}r(1-s_2)\sin\gamma \\ & - \frac{r\ddot{\alpha}_2(1-s_2) - r\ddot{\alpha}_1(1-s_1)}{H}(I_R + 2I_z + 2mH^2)\frac{r(1-s_2)}{H} + I_x\ddot{\alpha}_2 \\ & = M_{n2} + \left(-\frac{1}{2}P_u - \frac{1}{2}F_D - \frac{1}{2}G\sin\gamma + \frac{1}{2}F_w\sin\gamma - \frac{1}{2}W_{t2}\right)r(1-s_2) + M_p\frac{r(1-s_2)}{H} \end{aligned}$$

where r denotes the radius of the track drive sprocket, α_1 – angle of rotation of sprocket 1, α_2 – angle of rotation of sprocket 2, m_R – mass of the frame, m – mass of the track, W_t – rolling friction force, P_u – pull force, F_w – buoyant force, F_D – hydrostatic resistance force, M_{n1}, M_{n2} – torque on the drive sprockets of tracks 1, 2, H – distance between the tracks, I_R – moment of inertia of the robot frame, I_X, I_Z – reduced moments of inertia of the track drive

module, M_P – moment of transverse resistance, s_1 – slip of sprocket 1, s_2 – slip of sprocket 2, G – gravity force, η – efficiency.

Dynamic equations of motion (4.20) may be used to solve simple and inverse dynamics problems, however care must be taken when calculating values of the forces, particularly the rolling friction force W_t as various surfaces on which the robot operates would introduce significant variations in its value. The type fluid in which the robot moves has also strong influence on the forces, especially F_D and M_P .

5. Multibody simulations

Multibody simulations that aimed on the determination of torques of the positioning drives were performed using a simplified model of the robot. Imposed motion was defined for three drives by time dependent position input graphs corresponding to various possible positions of the track with respect to the robot body. Consecutive simulation steps are presented in Fig. 4.

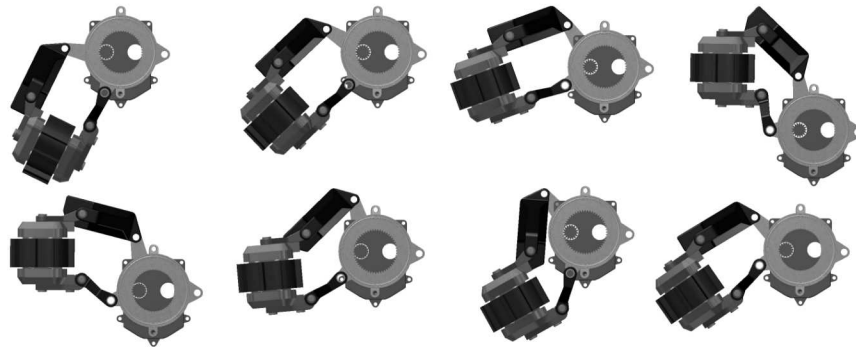


Fig. 4. Simulation – track positions

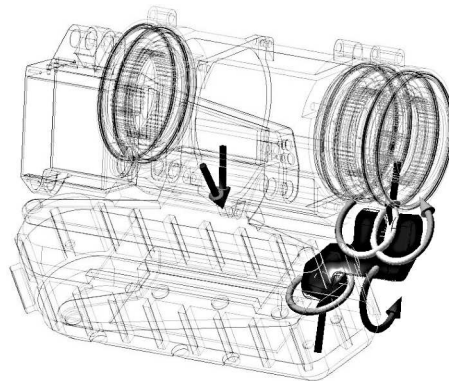


Fig. 5. Inner arm with imported loads from dynamic simulation

Three simulations using the same trajectory were performed. The first one involved lifting the track and orienting it in space with respect to the stationary robot body oriented horizontally. The second simulation involved vertical operation of the robot, where the extension forces exerted by the tracks on the pipe were assumed to be equal to the maximum track payload. In the third simulation, the maximum payload forces were applied to the tracks, whereas the gravity was acting downwards the robot body.

The results of simulations indicate that the torques in the arm drives do not exceed 3.6 Nm, whereas in the body drives 2 Nm. The results of simulations were used to select servomotors and optimize the geometry of the robot positioning system.

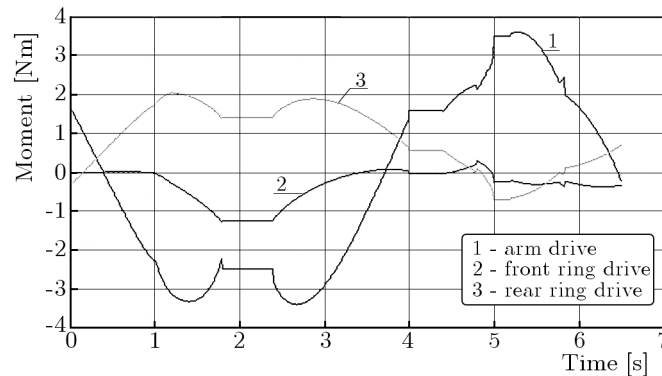


Fig. 6. Multibody simulations – drive torques in vertical operation

6. Operation environments

According to the project requirements, the robot is capable of positioning its driving mechanism in various ways to accommodate to the work environment. For the most compact alignment, the robot will be able to operate in pipes with diameter greater than 210 mm (Fig. 7). In Fig. 7, we may observe the robot with alignment for operation in a 350 mm diameter pipe. The upper limit of the pipe diameter is determined by the capabilities of the vision system.

The robot may also operate in pipes and ducts with a rectangular cross-section. The minimum width of a pipe is 230 mm (Fig. 7). As in the case of pipes with a circular cross-section, the maximum size is dependent on the capabilities of the mounted camera and lighting.

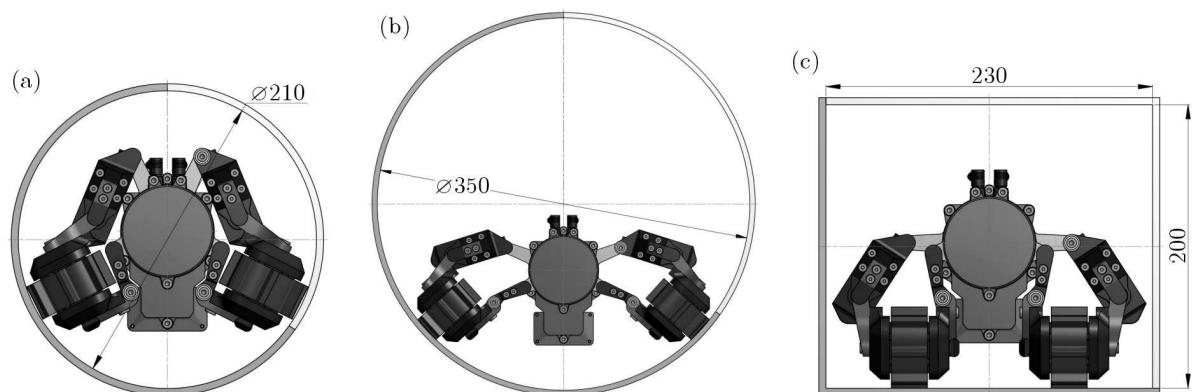


Fig. 7. Operation environments: (a) pipe $\varnothing 210$ mm, (b) pipe $\varnothing 350$ mm, (c) rectangular duct 230 mm wide

A parallel extension of tracks would be also achievable for the robot structure. It may be used to operate in pipes or ducts with rectangular or circular cross-sections that are oriented in any direction, based on friction forces with respect to the walls. Possible minimum and maximum extensions (230 mm to 270 mm) are presented in the Figs. 8a-d.

7. Simulations of the Inuktun Microtracs in Abaqus software

To simulate motion of the track under loading conditions, dynamical equations of motion were used with parameters obtained from laboratory tests to create a finite element model. The constructed model is based on the assumption that there exists an uneven load distribution in contact with the ground along the track length. It is caused by tensioning the track by three rollers (Fig. 9a).

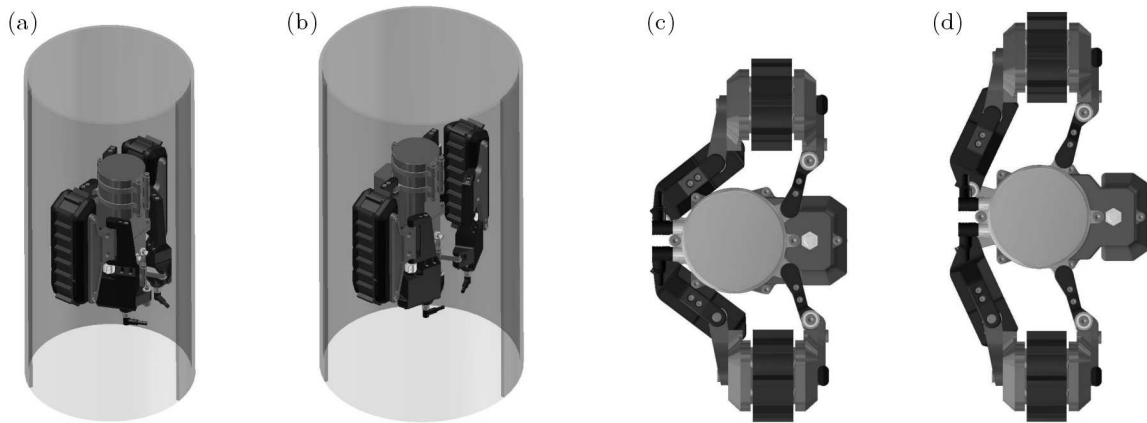


Fig. 8. Operation in vertical pipes: (a) $\varnothing 225$ mm, (b) $\varnothing 270$ mm; track parallel extension: (c) minimum, (d) maximum

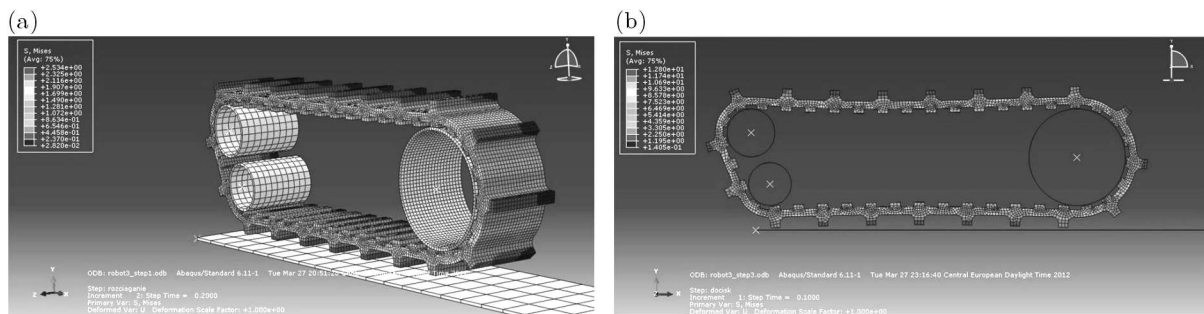


Fig. 9. FEA Simulation of Inuktun Microtracs: (a) stresses – isometric view, (b) stresses – side view

We may observe that the highest stresses appear in the outermost treads and the other have a resultant deformation. The simulation will be used for preparation of the control system to introduce corrections of the positioning error.

8. Testing of the Inuktun Microtracs in the real environment

In the case of motion of such mobile platforms as the described robot, there appear problems with precise determination of the position and orientation due to deformations of track treads and work surface (Wong, 2010). In order to reduce this unwanted influence, the previously described mathematical model was utilized. In the model, it was assumed that the track treads deform and the surface is undeformable.

The test procedure was conducted in a laboratory with usage of a horizontal pneumatic table with a vibration isolation and the Phantom v9.1 camera with 2 megapixel resolution. The vision system was equipped with the TEMA Automotive software, dedicated to motion analysis, featuring automatic tracking and processing tools.

The object of investigation consisted of two Inuktun Microtrac units mounted to the test frame with dimensions and weight corresponding to the designed robot. Markers were placed on each track tread and on the track body. During motion, displacements in the axes x and y were obtained for particular treads with respect to the marker situated in the lower left corner of the table (Fig. 10a). In Fig. 10b, we may observe plots of the tread marker position in the Y axis. Basing on the region of the plot, when the investigated tread is in contact with the table (lower plot), the deformation was calculated to be $\Delta l = 0.02$ mm for rectilinear motion.

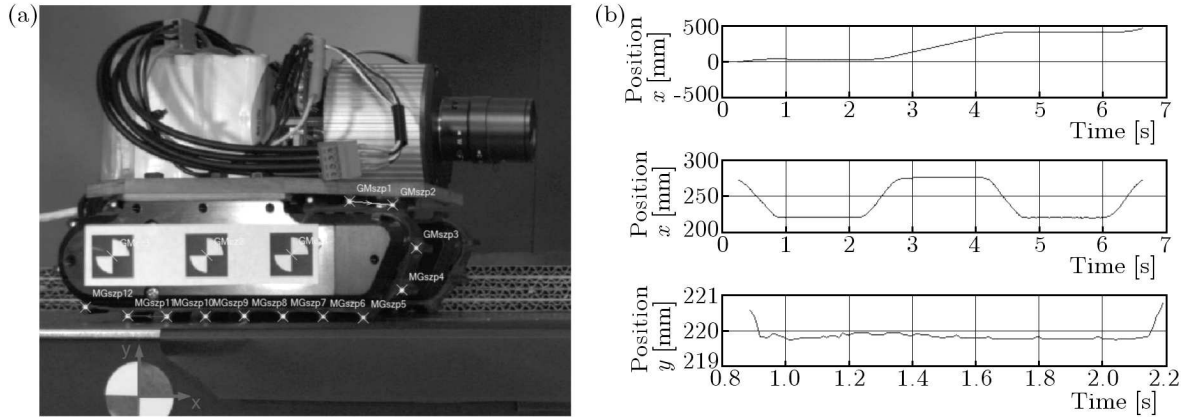


Fig. 10. Track deformation test – markers (a) and track tread position in the x and y axes

In order to validate dynamical equations of motion (4.20), a Matlab Simulink model (Fig. 11b) was prepared and simulated and a laboratory test was performed on the test platform. The rectilinear trajectory is presented in Fig. 11a.

Data used in the Matlab Simulink simulation: $r = 0.02794$ m, $H = 0.12$ m, $s_1 = s_2 = 0.011$, $P_u = 10$ N, $m = 1.1$ kg, $m_R = 3.04$ kg, $G = 51.404$ N, $I_R = 0.0194$ kg m², $I_Z = 0.000651$ kg m², $I_X = 0.000059$ kg m², $F_w = 18.639$ N, $\gamma = 0^\circ$, $\beta = 0^\circ$.

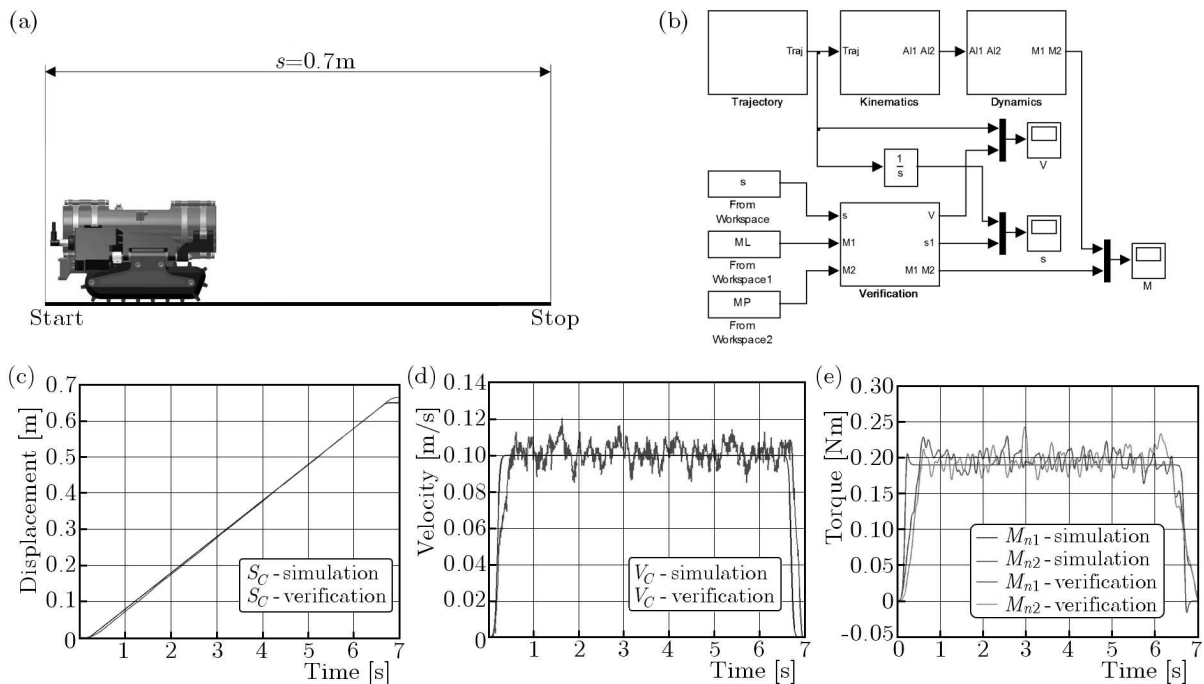


Fig. 11. Simulation and verification: (a) trajectory, (b) Matlab Simulink model structure, (c) displacement of point C , (d) velocity of point C , (e) track module drive sprocket torques

The results of simulation and verification are presented in Figs. 11a-c. We may observe that the calculated velocity and torques coincide considerably well with the measurements conducted on the test stand. In the results obtained from the verification, we may observe fluctuations of the velocity (Fig. 11b) and torques (Fig. 11c) caused by changes of contact of the track treads with the ground.

9. Conclusions

This project covers a design process of a pipe mobile inspection robot using CAD/CAE tools. By review of over 20 solutions, the market need for a tracked inspection robot with a flexible positioning mechanism was identified. A 3D model of a versatile mobile inspection platform was created and simulated. The potential work configurations of the robot were presented and motivated. Kinematic and dynamic mathematical models of the robot were formulated and verified experimentally.

10. Further work

Experiments with the track modules should be performed on different pipe and duct surfaces to provide values of the coefficient of friction that would allow estimation of proper loading for the positioning drives.

An efficient control system capable of on-line adaptation to the work environment must be created. The robot will be equipped with an Inertial Measurement Unit, and the control system should be developed based on the Kalman filter method presented by Buratowski *et al.* (2012). The prototype should be equipped with a CCTV camera and lighting to conduct further tests in the real operating environment. An algorithmic determination of the track treads deformation has to be developed, based on particular surfaces to optimize positioning of the structure in the work environment.

References

1. BURATOWSKI T., CIEŚLAK P., GIERGIEL J., UHL T., 2012, A self-stabilising multipurpose single-wheel robot, *Journal of Theoretical and Applied Mechanics*, **50**, 1, 99-118
2. BURDZIŃSKI Z., 1972, *Theory of Motion of a Tracked Vehicle* (in Polish), Wydawnictwa Komunikacji i Łączności, Warszawa
3. CHODKOWSKI A.W., 1982, *Modeling of Tracked and Wheeled Vehicles* (in Polish), Wydawnictwa Komunikacji i Łączności, Warszawa
4. CHODKOWSKI A.W., 1990, *Design and Calculations of High Speed Tracked Vehicles* (in Polish), Wydawnictwa Komunikacji i Łączności, Warszawa
5. CHOI H.R., ROH S., 2007, In-pipe robot with active steering capability for moving inside of pipelines, [In:] *Bioinspiration and Robotics Walking and Climbing Robots*, Maki K. Habib (Ed.), InTech, Vienna
6. Cues, 2012, Ultra Shorty III, <http://www.cuesinc.com/UltraShortyIII.html> [Accessed 24.04.2012]
7. DAJNIAK H., 1985, *Tractors, Theory of Motion and Design* (in Polish), Wydawnictwa Komunikacji i Łączności, Warszawa
8. GIERGIEL M., BURATOWSKI T., MAŁKA P., KURC K., KOHUT P., MAJKUT K., 2012, The project of tank inspection robot, *Key Engineering Materials*, **518**, 375-383
9. GIERGIEL J., ŻYLSKI W., 2005, Description of motion of a mobile robot by Maggie's equations, *Journal of Theoretical and Applied Mechanics*, **43**, 3, 511-521
10. HORODINCA M.H., DOROFTEI I., MIGNON E., PREUMONT A., 2002, A simple architecture for in-pipe inspection robots, *Proceedings of International Colloquium on Mobile and Autonomous Systems*, 61-64
11. Hydropulsion, 2012, Vertical Crawler Specification Sheet, <http://www.hydropulsion.com/robotic-crawler-systems/vertical-crawler/vertical.crawler.pdf> [Accessed 24.04.2012]

12. Inuktun, 2012, Inuktun crawler vehicles, <http://www.inuktun.com/crawler-vehicles> [Accessed 24.04.2012]
13. Ipek, 2011, ROVVER Brochure, http://www.ipek.at/fileadmin/FILES/downloads/brochures/iPEK_rovver_web_en.pdf [Accessed 08.03.2012]
14. Redzone, 2012, SOLO Unmanned Inspection Robot, <http://www.redzone.com/products/solo%C2%AE> [Accessed: 24.04.2012]
15. TADAKUMA K., TADAKUMA R., NAGATANI K., YOSHIDA K., MING A., SHIMOJO M., IAGNEMMA K., 2009, Basic running test of the cylindrical tracked vehicle with sideways mobility, *IROS 2009 IEEE/RSJ International Conference on Intelligent Robots and Systems*, St. Louis, 1679-1684
16. TROJNACKI M., 2011, Modeling and simulation of motion of a three-wheeled mobile robot taking into account wheels slippage (in Polish), *Modelowanie Inżynierskie*, **10**, 41, 411-420
17. WANG Y., ZHANG J., 2006, Autonomous air duct cleaning robot system, *MWSCAS'06. 49th IEEE International Midwest Symposium on Circuits and Systems*, **1**, 510-513
18. WONG J.Y., 2010, *Terramechanics and Off-Road Vehicle Engineering*, Butterworth-Heinemann, Amsterdam
19. ŻYLSKI W., 1996, *Kinematics and Dynamics of Wheeled Mobile Robots* (in Polish), Oficyna Wydawnicza Politechniki Rzeszowskiej, Rzeszów

Manuscript received March 14, 2013; accepted for print September 5, 2013